PCCP

Accepted Manuscript

ROYAL SOCIETY OF CHEMISTRY

www.rsc.org/pccp

Physical Chemistry Chemical Physics
CREATED USING THE RSC LaTeX PCCP ARTICLE TEMPLATE – SEE www.rsc.org/electronicfiles FOR DETAILS
ARTICLE TYPE www. rsc.org/xxxxxx | XXXXXXXX

Structural distortions in molecular-based quantum cellular automata: a minimal model based study†

Alejandro Santana Bonilla,*[a,b] Rafael Gutierrez,[a] Leonardo Medrano Sandonas,[a,b] Daijiro Nozaki,[a] Alessandro Paolo Bramanti,[c] and Gianaurelio Cuniberti[a,d,e]

Abstract

Molecular-based Quantum Cellular Automata (m-QCA), as an extension of quantum-dot QCAs, offer a novel alternative in which binary information can be encoded in the molecular charge configuration of a cell and propagated via nearest-neighbor Coulombic cell-cell interactions. Appropriate functionality of m-QCAs involves a complex relationship between quantum mechanical effects, such as electron transfer processes within the molecular building blocks, and electrostatic interactions between cells. The influence of structural distortions of single m-QCA are addressed in this paper within a minimal model using an diabatic-to-adiabatic transformation. We show that even small changes of the classical square geometry between driver and target cells, such as those induced by distance variations or shape distortions, can make cells respond to interactions in a far less symmetric fashion, modifying and potentially impairing the expected computational behavior of the m-QCA.

1 Introduction

Quantum Cellular Automata (QCA) have been proposed as a new and revolutionary paradigm for classical binary computing.[1] The basic computational unit, the QCA cell, consists of quantum dots connected in such a way as to allow both charge confinement on the dots and charge exchange between pairs of dots. Few (usually two) mobile charges can move between strongly localized electronic states. Bits of information (0 and 1) are then encoded by different geometrical arrangements of the charges within the cell. Information transfer between cells occurs via nearest-neighbor Coulomb interactions, i.e. no current flows from cell to cell, which dramatically reduces the power consumption of the device.[2]

In general, the charges will arrange so as to minimize the electrostatic energy which, for each cell, depends also on the charge configuration of neighboring cells. In the molecular version of QCA, the molecular-based QCA (m-QCA), quantum dots are implemented by moieties carrying localized electronic states, i.e. redox centers capable of accepting and donating electrons (reduction and oxidization respectively).[3] The redox centers are usually connected by bridging ligands determining the degree of localization of the charge carriers and acting as effective tunnel barriers.[4] Likewise, the electronic structure of the bridge defines the regime where the electron transfer occurs (hopping or super-exchange processes) and, consequently, the electron transfer rates (ET).[5] The choice of the redox centers and bridges are the knobs for fine chemical tuning of the QCA response.

In fact, a complex relationship arises between quantum mechanical effects (such as ET) and classical forces (electrostatic interactions between cells), which compete in determining the equilibrium between charge localization, necessary for the storage of readable states, and charge transfer, necessary for state switching and then, ultimately, for computation. In spite of the complexity of this process, some minimal models have been suggested, where a connection between the ET process and intermolecular interactions has been established using the diabatic-to-adiabatic transformation (DTA).[6,7]The same models allow defining a response function in which the ET coupling matrix element and the geometry of the system are effective parameters used to quantify the switching behavior necessary for the implementation of the QCA.[6]

However, while classical QCA configurations have been investigated quite deeply, what is the effect on computation of real-world asymmetries is still under debate and is a crucial point in order to understand the boundaries of applicability of the m-QCA paradigm.[8–19]

In particular, QCA are based on the tacit assumption that the cell configuration is perfectly square (in the case of four-dot cells) and identical for all cells, a condition which is hardly met in real-world systems, even more so at the molecular scale, where thermal fluctuations or structural defects make it hard even to consider a static geometry. Based on minimal m-QCA single cell models, we address in this work the influence of structural distortions of individual m-QCA cells on their response function. The basic approach, introduced in Sec.2 relies on previous studies by Lent and co-workers,[6] but is ex-

[a] *Institute for Materials Science and Max Bergmann Center of Biomaterials, Dresden University of Technology, 01062 Dresden, Germany*
[b] *Max Planck Institute for the Physics of Complex Systems, 01187, Dresden, Germany.*
[c] *STMicroelectronics Srl, Distretto Tecnol, I-73100 Lecce, Italy.*
[d] *Center for Advancing Electronics Dresden, Dresden University of Technology, 01062 Dresden, Germany.*
[e] *Dresden Center for Computational Materials Science, Dresden University of Technology, 01062 Dresden, Germany.*

tended to include conformational changes of the molecules. Our results strongly indicate that rather weak conformational changes may have a dramatic influence on the cell response of the m-QCA and hence, potentially undermining or, at least, deeply modifying the implementation of a m-QCA network with respect to the classical paradigm.

2 Theoretical modeling

2.1 Single-molecule QCA cell

In this study, we will consider the simplest m-QCA (half)cell represented by two quantum dots, which are separated by an effective tunnel barrier. The quantum dots represent the regions in the molecule where a charge can be localized, while the tunneling barrier mimics the role played by the bridging ligands that links the redox centers.[6,20] As shown in Fig.1, the external driver molecule is simply built by two point charges, whose main function is to start the switching process in the second molecule (target molecule), in analogy to the external voltage source needed to set in the switching process in semiconductor quantum-dot QCA implementations.[8] Thus, for the driver molecule, one can define a quantity ($q_{1,2}$) that represents the excess in the charge population that can freely move between the driver redox centers. In our case, the excess of charge is assumed to be one electron leading to the condition that $q_1+q_2=1$. In the case of the target molecule, the net population is related to the associated occupation probabilities in the (ground state) wave function, which follows the normalization condition ($|c_a|^2+|c_b|^2=1$). Within the diabatic-to-adiabatic transformation, the interplay between classical Coulombic interactions (driver-target) and quantum mechanical effects (ET process within the target) can be quantitatively described, as illustrated in the next section.

2.2 Diabatic to adiabatic transformation of the electronic states

To describe intra-molecular electron transfer (ET) processes, the simplest approach relies on a two-state approximation, taking as a reference point the localized diabatic states representing initial and final stages of the ET process.[4] For a minimal m-QCA model containing only two redox centers, the corresponding Hamiltonian matrix can then be written as:

$$\begin{bmatrix} H_{aa} & H_{ab} \\ H_{ba} & H_{bb} \end{bmatrix} \begin{bmatrix} c_a \\ c_b \end{bmatrix} = E \begin{bmatrix} c_a \\ c_b \end{bmatrix}, \quad (1)$$

where $H_{aa}=\langle\phi_a|H|\phi_a\rangle$, $H_{bb}=\langle\phi_b|H|\phi_b\rangle$ and $H_{ab}=H^*_{ba}=\langle\phi_a|H|\phi_b\rangle$. The corresponding eigenfunctions (diabatic states) for H_{aa} and H_{bb} are denoted by $|\phi_a\rangle$ and $|\phi_b\rangle$ with associated eigenvalues E_a and E_b, respectively. The overlap $\langle\phi_a|\phi_b\rangle$ between the diabatic states is neglected. The H_{aa} and H_{bb} terms represent the situation where the excess of charge is localized either at the upper or lower part of the target molecule, and can be considered as the initial and final stages of the ET process, respectively. These matrix elements include the influence of the driver and, since the charge is fully localized in those states, H_{aa} and H_{bb} can be computed using classical electrostatics. For the fully symmetrical case, where $d=L$, see Fig.1(a), the result is simply:[6]

$$\begin{aligned} H_{aa} &= \frac{e^2}{4\pi\varepsilon_0}\left[\frac{q_1}{L}+\frac{(1-q_1)}{2\sqrt{L}}\right], \quad (2)\\ H_{bb} &= \frac{e^2}{4\pi\varepsilon_0}\left[\frac{q_1}{\sqrt{2}L}+\frac{(1-q_1)}{L}\right]. \end{aligned}$$

The H_{ab} and H_{ba} matrix elements can be then understood as the quantum mechanical mixing between the two-electronic diabatic states. Diagonalizing the Hamiltonian is straightforward and the corresponding eigenvalues are given by: $2E_\pm = H_{aa}+H_{bb}\pm\sqrt{(H_{aa}-H_{bb})^2+4H^2_{ab}}$. Furthermore, from the adiabatic solutions, one can find the coupling between diabatic states at the degeneracy point ($H_{aa}=H_{bb}$) as:

$$\gamma = H_{ab} = \frac{E_+ - E_-}{2}. \quad (3)$$

We will only consider the super-exchange regime for ET, where the donor-acceptor charge transfer takes place via a tunneling process, with no population of the bridge states. In the super-exchange regime, we can write γ as an exponential function of the donor-acceptor separation R:

$$\gamma = \gamma_0 e^{-\alpha R}, \quad (4)$$

where α is system-dependent. Notice that in general the coefficient α includes information about the energetics of the bridge states, e.g. as in the McConnell formula,[21] but since the atomistic details of the bridge are not explicitly included in our model approach, we will not further discuss this issue here. If not stated otherwise (see Sec. 2.3.2), the reference values for the electronic coupling elements are listed in Table (2), see also Ref[6].

Table 1 Typical reference parameters used in Eq. 4 for the two studied molecule types[6,22]

Complex	$\alpha(nm^{-1})$	$\gamma_0(eV)$	γ(eV)
1,4-diallyl butane	4.66	6.68	
allyl-$(CH_2)_3$-allyl			0.52
allyl-$(CH_2)_9$-allyl			0.0119
diferrocenylpolyenes	0.84	0.12	
FC-1-FC			0.061
FC-5-FC			0.028

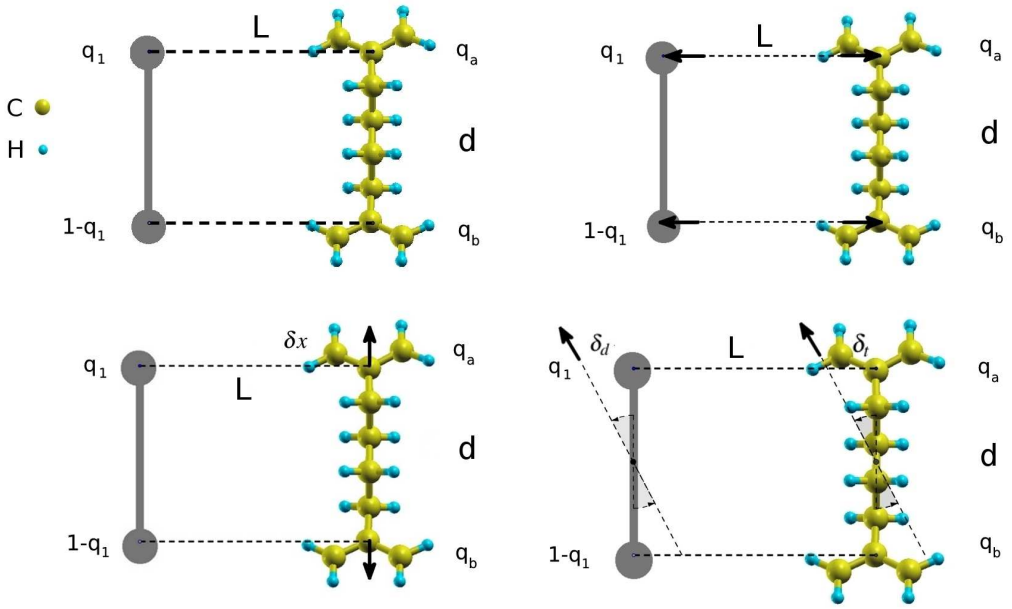

Fig. 1 Schematic representation for the driver-target configurations studied in this article. Only the case of the Aviram molecule (1,4-diallyl butane) is shown, for the ferrocene-based compound a similar representation holds. The driver molecule is represented by two partial charges q_1, q_2 such that $q_1 + q_2 = 1$, and separated by a distance d. The electric field of the driver induces a switching process in the target, which in general depends on the global geometric conformation of the system as well as on different electronic coupling parameters. Upper panel left: Symmetrical situation where both components are static. Upper panel right: The driver molecule is allowed to move along a line perpendicular to the axis of the target. Bottom panel left: Stretching and compression of the target molecule by δx that only affect the lenght of the bridge. Bottom panel right: Coordinated rotations between the driver and the target. In the small anngle approximation, the angular distortions can be related to the linear displacements δ_d and δ_t of the driver and target molecules, respectively.

2.3 Response function

In order to quantify the efficiency of a candidate molecule for its implementation in a m-QCA cell, a quantity needs to be defined that relates the cell response to an external driver. In particular, a well-defined switching between two states should take place in order to efficiently encode the two bits 0 and 1. These two states are related to charge reorganization inside the target cell under the action of the driver molecule. Such processes can be related to a polarization function, defined by $P_2 = \mathrm{Tr}\{\rho_t \sigma_3\} = |c_a|^2 - |c_b|^2 = 2|c_a|^2 - 1$. Here, ρ_t is the density matrix of the target and $\sigma_3 = diag(1,-1)$ is a Pauli matrix. Within the two-state approximation, the $c_{a,b}$ are the coefficients of the expansion of the ground state wave function in the diabatic basis. The corresponding polarization for the (classical) driver is then simply $P_1 = q_1 - q_2 = 2q_1 - 1$.

Using the adiabatic energy eigenvalues $E_\pm$, the expansion coefficient can be written as $c_a^2 = \gamma^2/(\gamma^2 + (E_+ - H_{aa})^2)$. After some simple manipulations,[6] the target polarization P_2 can be expressed as a function of the driver polarization P_1 as:

$$P_2 = \frac{2}{1 + \{\beta P_1 + \sqrt{(\beta P_1)^2 + 1}\}^2} - 1, \qquad (5)$$

with

$$\beta = \frac{e^2}{4\pi\varepsilon_0}\left[\frac{2-\sqrt{2}}{2}\right]\frac{1}{\gamma L}. \qquad (6)$$

Notice that the parameter β encodes information on both the electronic properties of the target (γ) and geometrical features of the problem (L). This expression was derived in Ref.[6] for a fully symmetric geometry ($d = L$). It is however of interest to address the problem of how resilient the system will be with respect to static (and dynamic, thermally induced) distortions of this ideal conformation, since such scenarios may be expected in real m-QCA networks. In what follows, we consider some basic geometrical distortions and how do they influence the polarization function P_2.

2.3.1 Relative translations between the driver and the target. The simplest modification will be to allow for a change in the linear driver-target distance. The driver is thus translated along a line perpendicular to the molecular axis as shown in Fig.1(a), where we define L as the distance between molecules and d the distance between redox/acceptor centers in the target molecule. Varying the driver-target distance will clearly affect the polarization switching of the target, since it determines the relative position of the diabatic states and

whether they will display a crossing point (or anti-crossing if speaking in terms of adiabatic states). The corresponding diabatic states for an arbitrary separation between target and driver L($\neq d$) is:

$$\begin{aligned} H_{aa} &= \frac{e^2}{4\pi\varepsilon_0}[\frac{q_1}{L}+\frac{(1-q_1)}{\sqrt{L^2+d^2}}], \\ H_{bb} &= \frac{e^2}{4\pi\varepsilon_0}[\frac{q_1}{\sqrt{L^2+d^2}}+\frac{(1-q_1)}{L}]. \end{aligned} \quad (7)$$

Along similar lines as in the previous section, the response function can be recast as:

$$P_2 = \frac{2}{1+\{\beta^* P_1+\sqrt{(\beta^* P_1)^2+1}\}^2}-1, \quad (8)$$

where now

$$\beta^* = \frac{e^2}{4\pi\varepsilon_0}\frac{1}{\gamma L}[1-\frac{1}{\sqrt{1+(\frac{d}{L})^2}}]. \quad (9)$$

Clearly, for the case $d = L$ we recover Eq. (6). For $d/L \ll 1$ the β^*-parameter scales as $\beta^* \sim (d^2/L^3)$ and the corresponding polarization as $P_2 \sim (1/L)(d/L)^2 P_1$, i.e. becomes asymptotically insensitive to the driver polarization P_1, as expected. In the opposite case ($d/L \gg 1$), $\beta^* \sim (1/L) \sim \beta$.

2.3.2 Elongations in the target molecule. The next possible distortion of the ideal driver-target geometry is a mismatch between the lengths of the driver and of the molecule. Denoting by δx (positive and negative) the stretching of the target length d (keeping the length of the driver constant and equal d), the diabatic matrix elements read:

$$\begin{aligned} H_{aa} &= \frac{e^2}{4\pi\varepsilon_0}[\frac{q_1}{\sqrt{L^2+\delta x^2}}+\frac{(1-q_1)}{\sqrt{L^2+(d+\delta x)^2}}], \\ H_{bb} &= \frac{e^2}{4\pi\varepsilon_0}[\frac{q_1}{\sqrt{L^2+(d+\delta x)^2}}+\frac{(1-q_1)}{\sqrt{L^2+\delta x^2}}], \end{aligned} \quad (10)$$

and the corresponding polarization becomes:

$$P_2 = \frac{2}{1+\{\beta^{**} P_1+\sqrt{(\beta^{**} P_1)^2+1}\}^2}-1, \quad (11)$$

with the new effective parameter

$$\beta^{**} = \frac{e^2}{4\pi\varepsilon_0}\frac{1}{\gamma L}[\frac{1}{\sqrt{1+(\frac{\delta x}{L})^2}}-\frac{1}{\sqrt{1+(\frac{d+\delta x}{L})^2}}]. \quad (12)$$

2.3.3 Angular distortions. The last, more involved, static distortions we are going to study, are in- and out-of-phase concerted motions of the driver and the target. In Fig.1(d) we schematically illustrate this situation, where both, target and driver molecules with length d rotate about their corresponding center-of-mass. We will limit our discussion to small angular distortions of size $\theta_{t,d}$ such that $\sin\theta_{t,d} \approx \theta_{t,d} = 2\delta_{t,d}/d$, with t, d denoting the target and driver distortions, respectively. In this limit, θ was expressed in terms of the linear displacements δ_t, δ_d and the diabatic states are found to be:

$$\begin{aligned} H_{aa} &= \frac{e^2}{4\pi\varepsilon_0}[\frac{q_1}{(L-\delta_d-\delta_t)} \\ &+ \frac{(1-q_1)}{\sqrt{(L+\delta_d+\delta_t)^2+(d^2-4\delta_t^2)}}], \\ H_{bb} &= \frac{e^2}{4\pi\varepsilon_0}[\frac{q_1}{\sqrt{(L-\delta_d-\delta_t)^2+(d^2-4\delta_d^2)}} \\ &+ \frac{(1-q_1)}{(L+\delta_d-\delta_t)}]. \end{aligned} \quad (13)$$

The corresponding polarization function can be cast as:

$$P_2 = \frac{2}{1+\{(\beta_1 P_1+\beta_2)+\sqrt{(\beta_1 P_1+\beta_2)^2+1}\}^2}-1. \quad (14)$$

In contrast to linear deformations, small angular distortions lead to an additional term (β_2). The new parameters are given by:

$$\begin{aligned} \beta_1 = \frac{e^2}{4\pi\varepsilon_0}\frac{1}{2\gamma}[&\frac{1}{(L-\delta_d+\delta_t)}+\frac{1}{(L+\delta_d-\delta_t)} \\ &-\frac{1}{\sqrt{(L+\delta_d+\delta_t)^2+(d^2-4\delta_t^2)}} \\ &-\frac{1}{\sqrt{(L-\delta_d-\delta_t)^2+(d^2-4\delta_d^2)}}], \end{aligned} \quad (15)$$

$$\begin{aligned} \beta_2 = \frac{e^2}{4\pi\varepsilon_0}\frac{1}{2\gamma}[&\frac{1}{(L-\delta_d+\delta_t)}-\frac{1}{(L+\delta_d-\delta_t)} \\ &+\frac{1}{\sqrt{(L+\delta_d+\delta_t)^2+(d^2-4\delta_t^2)}} \\ &-\frac{1}{\sqrt{(L-\delta_d-\delta_t)^2+(d^2-4\delta_d^2)}}]. \end{aligned} \quad (16)$$

In the previous equations, we have considered in general different distortions for the driver (δ_d) and the target (δ_t). However, to simplify the discussion we will consider in the following, if not stated otherwise, only symmetric cases where $|\delta_t| = |\delta_d| = \delta$. Notice however, that δ can still take both, positive and negative values. Based on this model, we can define two types of distortions: (i) in-phase displacements, where $sgn(\delta_t) = sgn(\delta_d)$, and (ii) out-of-phase displacements with $sgn(\delta_t) = -sgn(\delta_d)$.

3 Results

3.1 Single target molecule

In this section we will discuss the dependence of the target polarization function on the different geometrical distortions introduced in the previous sections and which are encoded in the different renormalized β-parameters. The main issue at stake is to which degree the strongly non-linear response of the target, required to guarantee a reliable QCA behavior, can be weakened or even destroyed by conformational distortions. Moreover, we will also address the differences in the molecular composition by comparing organic (diallyl butane) and diferrocenyl-based target molecules.

In Fig.2 the results are first presented for linear distortions and displacements in the driver-target configuration, for both, alkyl-diene and diferrocenyl based targets. The insets in all graphs refer always to longer bridges of the corresponding molecular system.

We remark at this point that the reference starting conformation for each of the cases presented in Fig. 2 is always that, where driver and target build a square with side length $L = d = d_{\text{bridge}}$, so that changes in the driver-target configuration (stretching, compression, separation) are performed assuming the allyl-$(CH_2)_n$-allyl molecules considered with both the short and long bridge $-d_{\text{bridge}}$ =0.54 nm and 1.35 nm, respectively. Similarly, d_{bridge}=0.7 nm (short bridge) and 1.63 nm (long bridge), for the Fc-n-Fc molecules. The corresponding electronic couplings for these reference configurations are listed in Table 2.

Let's first consider changes in the target-driver separation, as shown in the upper panel of Fig. 2. In all cases, we show the relative separation L/d_{bridge}, since absolute values are clearly very much dependent on the specific molecule type and conformation. The size of the L/d_{bridge} ratio will also strongly depend on its origin like mismatches in the assembly process. Since we are not addressing such issues in a realistic model, we consider different situations to show how they influence the cell response.

In the case of the carbon-only target molecules, Fig. 2(a), for short bridges, the non-linear response is rapidly suppressed for larger target-driver separations (~ 1.10 nm), since the contribution from the tunnel coupling $\gamma = 0.52$ eV is too large for short bridges, supporting charge delocalization and hence reducing the parameter β^* ($\beta^* \sim \gamma^{-1}$). Only for rather short driver-target separations the polarization function would recover its non-linear *S*-shape. For long bridges, see the inset of Fig.2(a), the non-linear dependence is largely preserved, since in this case the tunnel coupling is small enough, $\gamma = 0.012$ eV, to still guarantee charge localization on the redox centers.

Consider now the diferrocenyl-based molecules, Fig.2.(b). The first point to notice is that for both bridge lengths $n = 1$ and $n = 5$, the tunnel couplings are considerably smaller than for the carbon-based molecule allyl-$(CH_2)_n$-allyl: $\gamma = 0.061$ eV (short bridge) and $\gamma = 0.028$ eV (long bridge), see also Table 2. This suggests that the non-linear response of the target may be less sensitive to variations of the driver-target distance. This is clearly seen for the short Fc-1-Fc bridge, where the non-linear response is preserved except for the largest target-driver separation (1.40 nm). The relatively weak change of the tunnel coupling with increasing bridge length also implies that the polarization function does not strongly depend on the bridge length (compare with the inset of Fig.2.(b)).

Table 2 Changes in the electronic coupling γ upon stretching and compression of the target molecular bridge. The values of γ have been computed according to Eq. 4. All values are given in eV.

Molecule	$\gamma_{1\%}$	$\gamma_{-1\%}$	$\gamma_{10\%}$	$\gamma_{-10\%}$
allyl-$(CH_2)_3$-allyl	0.49	0.54	0.31	0.86
allyl-$(CH_2)_9$-allyl	0.0105	0.0136	0.00338	0.042
FC-1-FC	0.0670	0.0686	0.0602	0.0763
FC-5-FC	0.0303	0.0320	0.0237	0.0409

In the second case, introduced in Sec.2.3.2, we simulate possible linear distortions of the target molecule and investigate the influence of such distortions in the switching behavior for the m-QCA implementation. The results are shown in the lower panel of Fig.2, again for the carbon-only and the ferrocene based targets. Since now the length of the target molecule is changing, we compute the corresponding γ-coupling terms according to Eq. 4. Due to the assumed small ratio $\delta x/L$, the influence of such distortions turns out to be less dramatic than changes in the target-driver separation. This is clearly the case for longer bridges, where the strong non-linear response is well preserved for distortions of up to ± 10 %. For shorter bridges, the most affected one is, as expected, the allyl-$(CH_2)_3$-allyl due to the rather (on average) large γ.

In general terms, elongations of the molecule on the order of $\pm 1\%$ are reasonable and supported by quantum molecular dynamics simulations, while the other values of $\pm$ 10% are extreme cases that have been treated for the only purpose of showing how strong a structural distortion may be in order to considerably perturb the non-linearity of the cell response.

The last issue to be addressed are coupled motions of the target-driver system, as presented in Sec. 2.3.3. As mentioned before, two types of collective motions will be considered here. Firstly, in-phase rotations, in which both molecules move in the same direction along the line connecting both molecular axis creating a back and forth movement. Secondly, out-of-phase rotations, where one of the $\delta_{t,d}$ variables is taken negative, while the second one is chosen positive (although with the same absolute value). The results shown in Fig. 3 are all obtained for the special case $L = d/2$; the main qualitative features to be discussed below are similar for other separa-

tions between the target and the driver (as far as a switching is possible). The main influence of angular distortions is to shift the target polarization along the P_1-axis in a way that sensitively depends on the type of the considered collective distortions (in- or out-of-phase). This clearly induces a strong perturbation of the QCA response function. The value of P_2 at zero driver polarization is related to the β_2 parameter as $P_2 = 2/(1+\{\beta_2+\sqrt{(\beta_2)^2+1}\}^2)-1$, so that as long as β_2 does not vanish, a non-zero, topology-induced, residual polarization will exist and thus the target polarization displays a lag w.r.t. the driver. Hence, an additional field may be necessary to reset P_2 to zero in order to preserve the appropriate response of the target molecule in presence of static angular distortions. The strongest modifications of the polarization are found to occur for the out-of-phase distortions, which can induce a strong shift for angular displacements of the order of $\theta = \pm 7^\circ$. Our choice of relatively large angular distortions aims at illustrating in a clear way their effect on the cell polarization. In real molecular systems we may expect in general smaller angular distortions; their influence should be most likely noticeable for situations where no strong covalent bonding to the substrate takes place or when the active molecular species are attached to the substrate via longer inert linkers, which might increase the mechanical flexibility of the system. This latter case may be more realistic, since a good electronic decoupling from the substrate may turn out to be important in order to preserve the charge bi-stability of the mQCA cells.

The sensitivity on the relative phase of the distortions can be qualitatively understood by looking at the behavior of the β_2 parameter in the limit of $|\delta/(d/2)| \ll 1$. For in-phase motions ($sgn(\delta_t) = sgn(\delta_d)$), we get $\beta_2 \sim -(1/\gamma L)(1+(d/L)^2)^{-3/2}(\delta/L)$, while for the out-of-phase motion ($sgn(\delta_t) = -sgn(\delta_d)$), $\beta_2 \sim (1/\gamma L)(\delta/L)$. Hence, this correction has different signs depending on the type of distortion and it is easy to realize that the shift in P_2 (at $P_1 = 0$) will be stronger for the out-of-phase displacements.

So far, different types of static deformations have been treated. Angular distortions have turned out to have the strongest impact on the cell polarization. The influence of (small angle) thermal fluctuations is however more difficult to assess without computing in detail the vibrational spectrum of specific mQCA candidates, also taking into account the way such molecules would be attached to substrates, since this will clearly influence their mechanical degrees of freedom. To catch, at least in a qualitative way, the influence of small angle fluctuations, we have performed additional calculations to include the effect of thermal fluctuations of both, the driver and the target molecules. For this purpose, we have assumed now the displacements δ_d, and δ_t in Eqs. 15 and 16 to be random variables with a Gaussian distribution with zero mean and a variable width σ taking values up to 3°. Moreover, we do not consider in- or out-of-phase movements separately, but subsume them in the random fluctuations. In Fig.4 we show the results only for the longer bridges, since the behavior for shorter bridges is qualitatively similar. First of all, the strong shift of the polarization function along the P_1 axis, found in the case of static distortions, is now averaged out already for rather small fluctuations, so that the response function vanishes at $P_1 = 0$. This result can be understood by looking at the expression for zero driver polarization in the case of static disorder, $P_2 = 2/(1+\{\beta_2+\sqrt{(\beta_2)^2+1}\}^2)-1$. This function is odd with respect to a change in the sign of β_2, so that it vanishes when performing a conformational average over a Gaussian distributed disorder with zero mean. We also see in Fig.4 that with progressive increase of the disorder fluctuations (roughly equivalent to an increase of temperature, since we may expect $\sigma \sim k_B T$), the switching behavior is smoothed and rapidly becomes linear for $|P_1| \leq 0.5$. Assuming weak thermal disorder, it is possible to show that the configurational averaged slope $<\eta> = <dP_2/dP_1|_{P_1=0}>$ can be written as $<\eta> = g(\beta_2)\beta_1$, where $g(\beta_2)$ is a rational function of β_2 alone. Making the (rough) assumption that the fluctuations of the stochastic variables β_1 and β_2 are approximately independent, we can write after some simplifications the analytical result: $<\eta> \sim -<\beta_1>(1-(3/2)<\beta_2^2>)$. Since $<\eta>$ is always negative, this shows that the slope will be reduced with increasing fluctuations, i.e. with increasing temperature. However, the condition $<\beta_2^2> \leq 2/3$ needs to be fulfilled to make the approximation meaningful. This is guaranteed by the assumption of weak fluctuations.

3.2 *Validating the minimal model: first-principle calculations*

It is desirable to validate the results obtained using the previously introduced minimal models using some simple molecular system. Mainly the influence of static angular distortions needs to be further clarified. We have thus performed first-principle based calculations of the 1,4-diallyl butane radical cation using the density-functional tight binding code including self-consistent charge calculations (SCC-DFTB)[23–25] as well as dispersion interactions.[26] In this approach, a minimal valence basis set is used to represent the molecular orbitals within a LCAO approximation. Likewise, charge redistribution is taken into account through the incorporation of a self-consistent scheme for Mulliken charges based on a second-order expansion of the Kohn-Sham energy functional in terms of charge density fluctuations. As starting point, a dipole driver has been placed parallel to the 1,4-diallyl butane radical cation in order to maintain the same geometrical configurations used in our minimal models. As previously indicated, the total charge of the driver is 1 and we plot the variation of the molecular orbitals of the target while varying the driver polarization P_1. To provide a mobile charge in

the system, we consider the molecular cation, where an electron has been removed from the lower allyl-group leading to a situation where the anti-bonding level is singly occupied in the upper group and non-occupied in the lower allyl group. Charge transfer is expected, since the localized electron at the lower allyl-group can occupy one of the non-bonding levels at the opposite allyl-end group as it has been already demonstrated.[27] In our approach, for a given configuration of the driver polarization P_1 ranging from -1 to 1, the molecule is allowed to relax by using the conjugate gradient algorithm until the root mean square force was less than or equal to 10^{-4} a.u. Since the point charges on the driver induce an effective force on the molecule, the carbon atoms located at the center of each of the allyl-end groups are maintained fixed. In Fig.5, the HOMO and LUMO energy levels for the molecule are plotted as a function of the driver polarization P_1 for the case of out-of-phase rotations by 7 degrees.

At this point, we remark that in general terms, the switching of the target polarization while smoothly (adiabatically) varying the driver polarization takes place around the anti-crossing region of the adiabatic states (or at the crossing point of the diabatic states). In a real molecule, these states can be related to the HOMO and LUMO frontier orbitals. This picture is similar to a Landau-Zener[28] interpretation of charge transfer: the effective (time-dependent) reaction parameters can be associated with the driver-target distance L and, once L is fixed, with the rate of change of the driver polarization. In the case of a square geometry with the driver-target distance being similar to the distance between the allyl groups, the anti-crossing point is found at zero driver polarization. Hence, the target response function also vanishes at $P_1 = 0$. However, in the case of angular distortions, a shift in the anti-crossing point is found, whose sign depends on the relative orientation of driver and target, compare the top and bottom panels of Fig.5, where the results for the two possible out-of-phase conformations are displayed. This means, the target polarization is non-vanishing at $P_1 = 0$, the target response shows a lag with respect to the driver, and this is just the effect found in the minimal model calculations for static angular distortions, see Fig.3 for comparison. Similar shifts were also found in the in-phase distortions (not shown), but they turn out to be smaller, also in qualitative agreement with the model results. We remark that the found shifts of the target polarization are not fully symmetric around the vertical axis $P_1 = 0$ as in the case of the model calculations. This apparently relates to the fact that the real molecular system has a full three-dimensional structure, so that there may may slight asymmetries in the relative orientation of driver and target.

4 Conclusions

Static geometric distortions and thermal fluctuations in m-QCA have been studied systematically with respect to their impact on the functional response of the cell. The current investigation suggests that conformational changes related to static distortions of an m-QCA network may have deeper implications in determining the response of a network and hence, potentially alter its functionality. Further investigations are however necessary in order to fully validate this statement. Any real-world implementation of these systems will have to account for these effects, estimating the potential distortions and evaluating their effect on the final digital machine.

5 Acknowledgments

A.S.B. and R.G thank A. Dianat for very helpful discussions. This work was partly funded by the EU within the project *Molecular Architectures for QCA-inspired Boolean Networks* (MolArNet, project nr. 318516). A.S.B. thanks the Max Planck Institute for the Physics of Complex Systems for financial support. This work has also been partly supported by the German Research Foundation (DFG) within the Cluster of Excellence "Center for Advancing Electronics Dresden". Computational resources were provided by the ZIH at the Dresden University of Technology.

References

1 C. S. Lent, *Science*, 2000, **288**, 1597–1599.
2 J. Timler and C. S. Lent, *Journal of Applied Physics*, 2002, **91**, 823–831.
3 C. Lambert, C. Risko, V. Coropceanu, J. Schelter, S. Amthor, N. E. Gruhn, J. C. Durivage and J.-L. Brdas, *Journal of the American Chemical Society*, 2005, **127**, 8508–8516.
4 T. Van Voorhis, T. Kowalczyk, B. Kaduk, L.-P. Wang, C.-L. Cheng and Q. Wu, *Annual Review of Physical Chemistry*, 2010, **61**, 149–170.
5 J.-P. Launay, *Coordination Chemistry Reviews*, 2013, **257**, 1544 – 1554.
6 Y. Lu and C. S. Lent, *Nanotechnology*, 2008, **19**, 155703.
7 E. Rahimi and S. M. Nejad, *Nanoscale Research Letters*, 2012, **7**, 1 – 13.
8 M. Macucci, in *Quantum Cellular Automata*, Wiley-VCH Verlag GmbH and Co. KGaA, 2010.
9 F. Rojas, E. Cota and S. E. Ulloa, *Phys. Rev. B*, 2002, **66**, 235305.
10 V. Arima, M. Iurlo, L. Zoli, S. Kumar, M. Piacenza, F. Della Sala, F. Matino, G. Maruccio, R. Rinaldi, F. Paolucci, M. Marcaccio, P. G. Cozzi and A. P. Bramanti, *Nanoscale*, 2012, **4**, 813–823.
11 N. A. Wasio, R. C. Quardokus, R. P. Forrest, S. A. Corcelli, Y. Lu, C. S. Lent, F. Justaud, C. Lapinte and S. A. Kandel, *The Journal of Physical Chemistry C*, 2012, **116**, 25486–25492.
12 I. Sturzu, J. Kanuchok, M. Khatun and P. Tougaw, *Physica E: Low-dimensional Systems and Nanostructures*, 2005, **27**, 188 – 197.
13 M. Crocker, X. S. Hu and M. Niemier, *J. Emerg. Technol. Comput. Syst.*, 2009, **5**, 1–27.
14 M. Crocker, M. Niemier, X. S. Hu and M. Lieberman, *J. Emerg. Technol. Comput. Syst.*, 2008, **4**, 1–21.
15 T. Dysart, *Nanotechnology, IEEE Transactions on*, 2013, **12**, 553–560.

16 A. Pulimeno, M. Graziano, A. Sanginario, V. Cauda, D. Demarchi and G. Piccinini, *Nanotechnology, IEEE Transactions on*, 2013, **12**, 498–507.
17 J. Huang, M. Momenzadeh, M. Tahoori and F. Lombardi, Defect and Fault Tolerance in VLSI Systems, 2004. DFT 2004. Proceedings. 19th IEEE International Symposium on, 2004, pp. 30–38.
18 M. T. Niemier and P. M. Kogge, *International Journal of Circuit Theory and Applications*, 2001, **29**, 49–62.
19 M. Ottavi, S. Pontarelli, E. DeBenedictis, A. Salsano, S. Frost-Murphy, P. Kogge and F. Lombardi, *Nanotechnology, IEEE Transactions on*, 2011, **10**, 1383–1393.
20 C. S. Lent, B. Isaksen and M. Lieberman, *Journal of the American Chemical Society*, 2003, **125**, 1056–1063.
21 A. Onipko, *Chemical Physics Letters*, 1998, **292**, 267 – 272.
22 A.-C. Ribou, J.-P. Launay, M. L. Sachtleben, H. Li and C. W. Spangler, *Inorganic Chemistry*, 1996, **35**, 3735–3740.
23 B. Aradi, B. Hourahine and T. Frauenheim., *J. Phys. Chem. A*, 2007, **26**, 5678–5684.
24 M. Elstner, D. Porezag, G. Jungnickel, J. Elsner, M. Haugk, T. Frauenheim, S. Suhai and G. Seifert, *Phys. Rev. B*, 1998, **58**, 72607268.
25 C. Köhler, G. Seifert and T. Frauenheim., *Chem. Phys.*, 2005, **309**, 23–31.
26 M. Elstner, P. Hobza, T. Frauenheim, S. Suhai and E. Kaxiras, *J. Chem. Phys*, 2001, **114**, 5149–5155.
27 C. S. Lent, B. Isaksen and M. Lieberman, *J. Am. Chem. Soc.*, 2003, **125**, 1056–1063.
28 A. Nitzan, *Chemical Dynamics in Condensed Phases: Relaxation, Transfer, and Reactions in Condensed Molecular Systems*, Oxford University Press, Oxford, 2006.

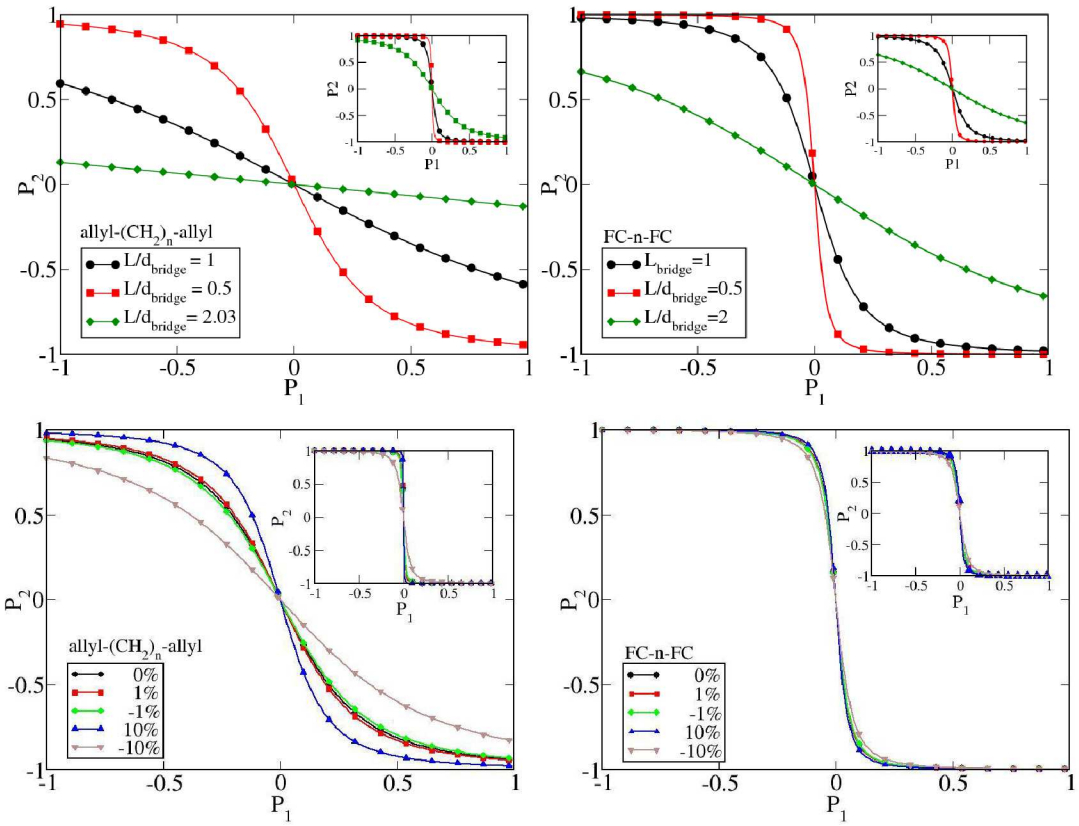

Fig. 2 Response function of the target molecule for driver-target translations (upper panel) and target elongations (lower panel). Results for both, alkyl-diene and diferrocenyl based molecules are shown. In all cases, the insets correspond to longer bridges separating the redox centers (n=9 for alkyl-diene and n=5 for diferrocenyl based molecules), see also Fig. 1. Driver-target separations are given in terms of the ratio L/d_{bridge}, while elongations of the target are given by d/d_{bridge} (%). Changes in the geometrical conformations lead to a renormalization of the β parameters and thus to a tuning of the target's response P_2 while varying the driver polarization P_1. Since in all cases the β parameters scale as γ^{-1}, short and long bridges display in general qualitatively different behaviors; this is especially the case for the alkyl-diene target, compare also with Table 2.

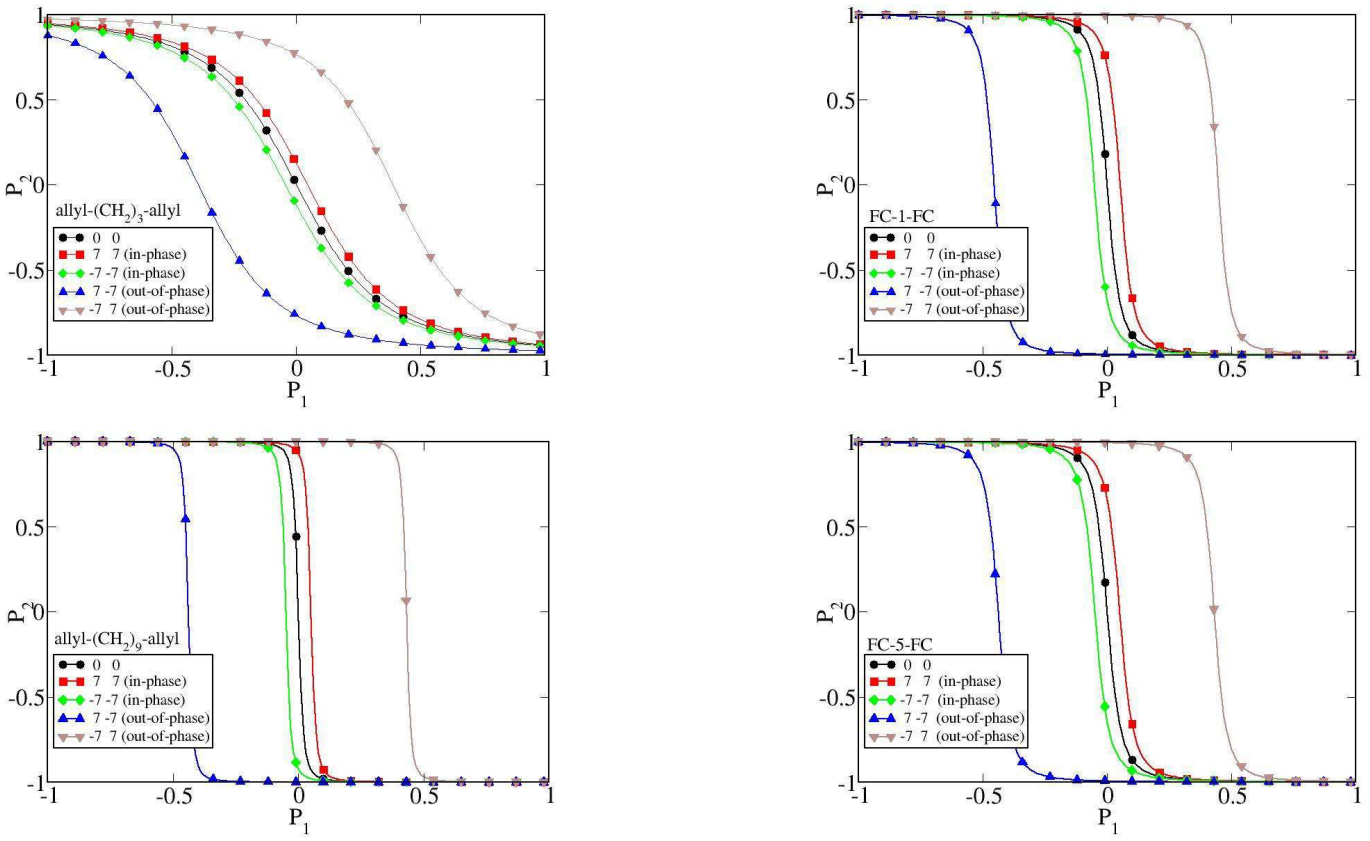

Fig. 3 Response function of the target molecule as a function of the driver polarization for the case of coupled angular distortions. Results for the alkyl-diene molecules with two different bridge lengths as well as for the diferrocenyl based systems are shown. The general notation θ_d, θ_t indicates the angular distortions (in degrees) of the driver (d) and target (t). As mentioned in the text, we assume for simplicity $|\theta_d| = |\theta_t| = \theta$. The differences in the signs correspond to two qualitative different situations: in-phase displacements of the target and the driver $(\theta(-\theta), \theta(-\theta))$, and (ii) out-of-phase displacements $(\theta(-\theta), -\theta(\theta))$. The main effect of the angular distortions is to induce a horizontal shift of the target's response function, so that a non-zero target polarization may appear even if the driver polarization is zero. Thus, even small angular displacements can dramatically destroy the required sstructure of the response function of the m-QCA.

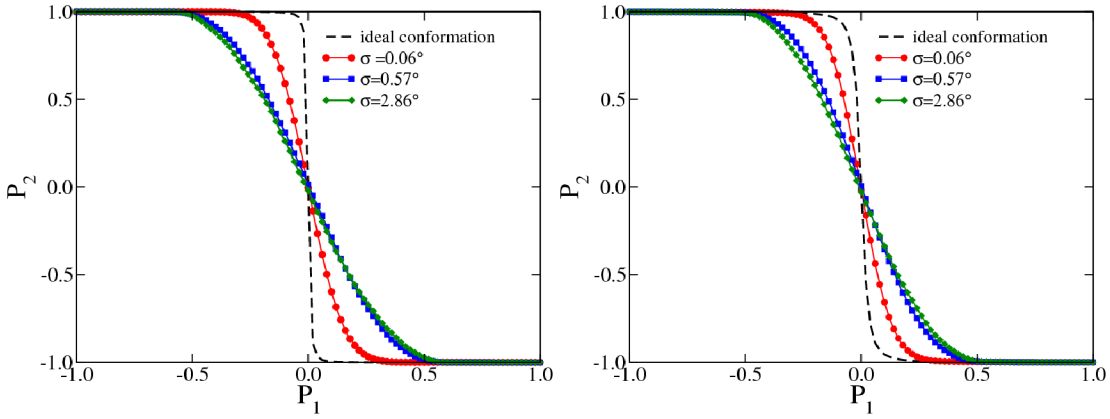

Fig. 4 Configurational average of the response function of the target molecule as a function of the driver polarization for different degrees of angular disorder. Only results for the longer molecular bridges of alkyl-diene and ferrocene based m-QCA are shown. The variance σ gives the width of the Gaussian distribution used to mimic thermal fluctuations in the angular distortions of both, the target and the driver. We note that no difference between in-phase and out-of-phase motion has been made, so that both driver and target are allowed to freely fluctuate around their parallel conformation. The only constrain is that the size of the fluctuations should still allow for a small-angle approximation used in deriving the corresponding analytic expressions for the parameters $\beta_{1,2}$. The strong shift in the target polarization found for static disorder, see Fig. 3, is now removed.

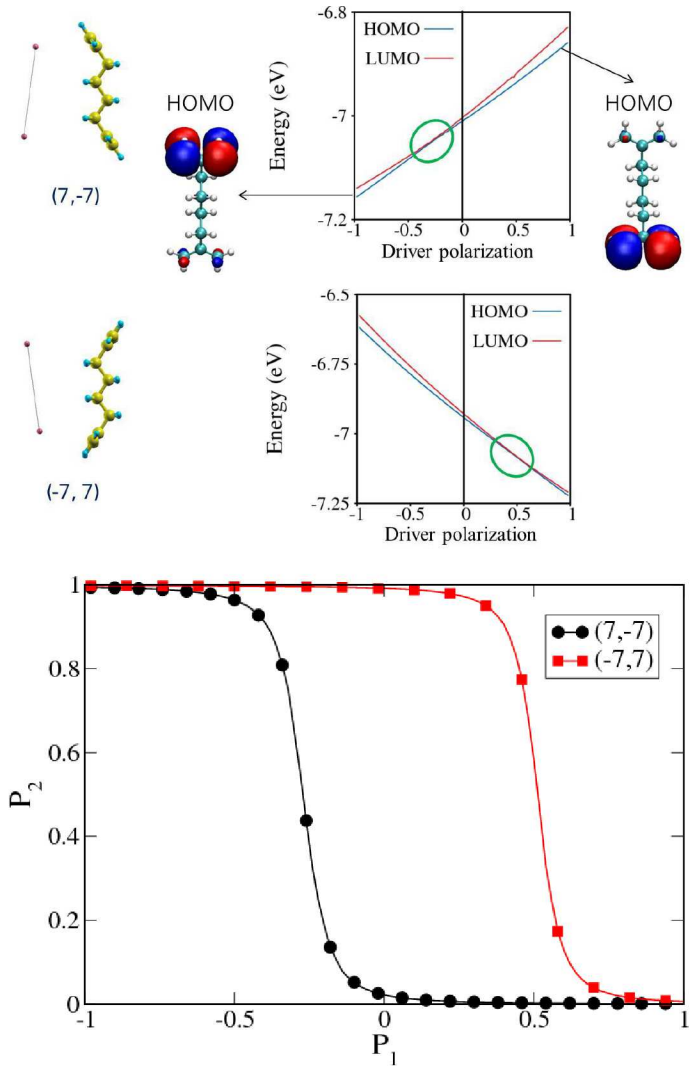

Fig. 5 Upper panel: Calculated HOMO and LUMO energy levels for the 1,4-diallyl butane radical cation where (out-of-phase) angular distortions of both target and driver are taken into account, see also Fig. 3. The angular distortions between driver and target are (a) (7,-7) and (b) (-7,7). Notice the shift (encircled) of the anti-crossing point of the molecular states to the left or right of the zero driver polarization in dependence of the relative angular distortion of the driver and target. The shifts are not fully symmetric, which is only reflecting the fact that the real molecular system is not fully planar. Also shown in the figure are the charge density plots of the HOMO state for the two limiting driver polarizations $P_1 = -1$ and $P_1 = 1$. Lower panel: Corresponding cell response function.